NANO · MICRO small
www.small-journal.com

Hybrid Triboelectric-Electromagnetic Magnetic Energy Harvester-Based Sensing for Wireless Monitoring of Transmission Lines

Zhihao Yuan, Xu Jin, Ruonan Li, Baocheng Wang, Chengcheng Han, Yapeng Shi, Zhiyi Wu, and Zhong Lin Wang*

Magnetic energy is an abundant and persistent form of energy radiating from various sources. Here, a hybrid triboelectric-electromagnetic magnetic energy harvester (HMEH) system consisting of a modified pendulum unit is proposed, interacting mechanically with two multilayered TENGs and remotely with Cu coils. Systematic studies are conducted on magneto-mechano-energy conversion from power transmission lines. The pendulum is made out of a thin PET plate, with two permanent magnets stuck at each side of the free end of the PET plate. Two multilayered TENGs (each of which has one layer fixed at the same angle while other layers are set free) are located at both sides of the pendulum unit. The coils and the magnets make up the electromagnetic generator (EMG). Multilayered TENGs are connected in parallel with the EMG (each unit is connected to an independent rectifying bridge), and it is possible to charge a 100 μF capacitor to 4.78 V within 55 s. The HMEH system is used to power up a thermometer continuously via a 47 μF capacitor. Furthermore, a design for a wireless early warning system for potential fire hazards due to overheating is realized, revealing potential applications for self-powered wireless monitoring of transmission lines.

1. Introduction

Emerging technologies in power systems such as smart grids and ubiquitous power internet of things have attracted considerable interest in recent years.[1,2] The operational condition perception of the transmission line in the grid and measurement of the grid parameters are critical for achieving system intelligence in power system construction.[3–5] Massive real-time information needs to be collected for condition monitoring, bringing forward a high request of the sensors. Sensors can meet part needs to detect transmission lines and reduce labor costs, which enable maintenance personnel to address potential risks in time.[6,7] However, a new problem of power source failure appears: the difficulty of replacing the battery for the facilities in remote areas. Consequently, energy harvesting technology is deemed a promising solution to power the monitoring system continuously.[8–10]

Nowadays, extensive research efforts have been dedicated to harvesting line energy based on building an energy harvester. Energy harvesting technology allows for generating electrical power from the surrounding environment, such as sunlight, heat, wind, wave and magnetic fields.[11–17] Magnetic energy is an available energy source because the stray magnetic field caused by the transmission line constantly exists. Triboelectric nanogenerators (TENGs) based on triboelectrification and electrostatic induction have gained extensive attention because of the merits of considerable design flexibility, simple structure, and low cost.[18–22] Several energy harvester prototypes based on the TENG have been developed to harvest stray magnetic energy. Huang et al. demonstrated a magneto-mechano-triboelectric nanogenerator (MMTENG) based on a cantilever beam and magnetic field responsive vibrating materials.[23] The MMTENG harvested energy from mechanical contact separation under stray magnetic fields, which has driven small electronics such as light-emitting diode indicators, thermometers and Bluetooth beacons.[24–27] However, the rigid cantilever beam limits the range of motion, conditioning the installation, and constraining the structure improvement. Also, the electromagnetic generator (EMG) can be attached to the moving part to convert magnetic energy into electrical energy and further increase the total power output.[28–31]

This work reports a hybrid triboelectric-electromagnetic magnetic energy harvester (HMEH) based on a flexible

Z. Yuan, X. Jin, R. Li, B. Wang, C. Han, Y. Shi, Z. Wu, Z. L. Wang
Beijing Institute of Nanoenergy and Nanosystems
Chinese Academy of Sciences
Beijing 101400, P. R. China
E-mail: wuzhiyi@binn.cas.cn
Z. Yuan, X. Jin, R. Li, Z. L. Wang
Center on Nanoenergy Research
School of Physical Science and Technology
Guangxi University
Nanning 530004, P. R. China
B. Wang, C. Han, Y. Shi, Z. L. Wang
School of Nanoscience and Technology
University of Chinese Academy of Sciences
Beijing 100049, P. R. China
Z. L. Wang
School of Materials Science and Engineering
Georgia Institute of Technology
Atlanta, GA 30332-0245, USA
The ORCID identification number(s) for the author(s) of this article can be found under https://doi.org/10.1002/smll.202107221.

DOI: 10.1002/smll.202107221

pendulum structure. It is employed as a power source for wireless monitoring of transmission lines. The TENG utilizing contact–separation mode is designed into a multilayered structure, enlarging the output current to some extent. The EMG is constituted of a copper coil and magnets. The magnets react to the alternative magnetic field, driving the TENG operation. They also serve as mass blocks, affecting the output performance of the TENG. The flexible and stretchable pendulum resembles an arc caused by the magnetic force, which acquires a big displacement. The performance of the TENG module and the EMG module was studied, and the capacitance charging rate was significantly higher than that of individual TENG or EMG. Moreover, the connections of the TENG and EMG modules were also investigated. A temperature alarm system has been established using a wireless transmitter and receiver under the parallel connection mode. This work proposes a strategy to harvest the magnetic energy of the transmission line, which is of great importance and can be an effective supplement for the current micro-energy structure.

2. Results and Discussion

2.1. Design and Working Principle of HMEH

Conducting transmission line patrols may be difficult in an inaccessible area, so sensors are a good alternative. The usage of sensors advances the power supply requirement, which the ambient energy harvester may be able to provide. **Figure 1**a illustrates and describes the magnetic energy harvester with a simple structure, and being low-cost it can be installed on transmission lines to power the sensors. Powered by the HMEH, the temperature information can be received by maintenance crews in time. Accordingly, the potential fire disaster will be strangled at birth. A coil-based EMG, a flexible pendulum, and two multilayered TENGs make up the HMEH device (Figure 1b). The coil is positioned at the device's base, abutting the magnets (NdFeB, N35) attached to the elastic beam's bottom. Two pairs of contact–separation mode TENGs make up the multilayered TENG unit. The substrate material is acrylic because of its superior mechanical strength, and foam enhances the contact between the two tribo-layers. Fluorinated ethylene propylene (FEP) film and Cu film are chosen as the composition of the charge transport layer due to their positive and negative electron affinities, respectively. The inclined TENG units limit the swing amplitude and increase the swing frequency of the flexible pendulum, which indirectly improves the output of the EMG unit. Figure 1d shows photographs of the multilayered TENG and Cu coil. In addition to the swing amplitude, there is also vibration amplitude, which reaches its maximum value when the upper edge of the multilayered TENG is positioned at half the height of the pendulum. The lower edge is located on the motion path of the pendulum to avoid the excessive swing amplitude of the pendulum.

Stress analysis can be found in Figure 1c, illustrating the motion state of the flexible pendulum. The magnets respond to the alternating magnetic field, providing motion inertia to the pendulum. They also play the role of mass blocks, further increasing the stress on the pendulum. The pendulum will vibrate because the direction of the magnetic force changes with the alternating magnetic field. Besides, the tension of the flexible pendulum brought by the magnets does not always follow the direction of the pendulum, which makes the length of the pendulum slightly deformed in the radial direction or even bent. Then the resultant force combined with gravity, tension, and magnetic force will drive the flexible pendulum to achieve a larger swing amplitude in a state of vibration (a comparison of motion states of flexible and rigid pendulums can be visualized in Video S1, Supporting Information). Both pendulums vibrate when the alternative magnetic field generator is just turned on. Then, the flexible one gradually starts swinging as described above, while the rigid pendulum only vibrates at the same frequency as the alternating magnetic field. Therefore, the output performance of a rigid and flexible pendulum is considerably different (Figure S1, Supporting Information). The negligible vibration amplitude in the case of the rigid pendulum results in smaller impulses, causing the TENG response to be affected only by the net acting force in a relatively shorter period of hitting time, unlike the extended hitting time in the flexible pendulum case. As a result, the output voltage obtained by the rigid pendulum is much smaller than the flexible one, while the waveform is more regular.

Figure 1e schematically illustrates the working mechanism of the HMEH. When the swinging pendulum drives the multilayered TENG to contact, the left Cu electrode and the right FEP layer are charged with positive and negative charges, respectively (Figure 1e-i). As the pendulum leaves the multilayered TENG, two tribo-layers separate, and the positive charges of the left Cu electrode flow to the right Cu electrode through the external circuit (Figure 1e-ii). Then, all positive charges transfer to the right Cu electrode (Figure 1e-iii) as the pendulum continues to move away. Finally, the positive charges flow in the opposite direction (Figure 1e-iv). The TENGs work continuously and generate an alternating current in an external circuit. Simultaneously, the EMG produces electricity according to the electromagnetic induction effect.

2.2. TENG Response of HMEH and its Optimization

Figure 2a shows simulation results by COMSOL software based on a simple model with an estimation of electric potential change for contact separation of the TENG unit (see Note S1, Supporting Information, for details). The source of voltage generation can be understood from the forces acting on the multilayered TENG unit by the swinging pendulum (described in Figure S2, Supporting Information), and the impulse varies in the different parts of the TENG unit, which are labeled as tribo-layers A, B, and C in Figure 2a-i. The impulse acts on the tribo-layer A of the TENG unit at the middle of the pendulum (Figure S2ii, Supporting Information), and the tribo-layer-A moves together with the tribo-layer B, which is followed by the motion of tribo-layers A and B toward the tribo-layer C making all tribo-layers in full contact (Figure 2a-ii) by the bottom end of the pendulum until the tribo-layer-A gets no support from the pendulum (Figure S2iii, Supporting Information). This is the moment the pendulum starts vibrating and stays in vibration mode (Figure 2a-iii), causing all tribo-layers to continuously tap each other while the varying tension force gradually diminishes

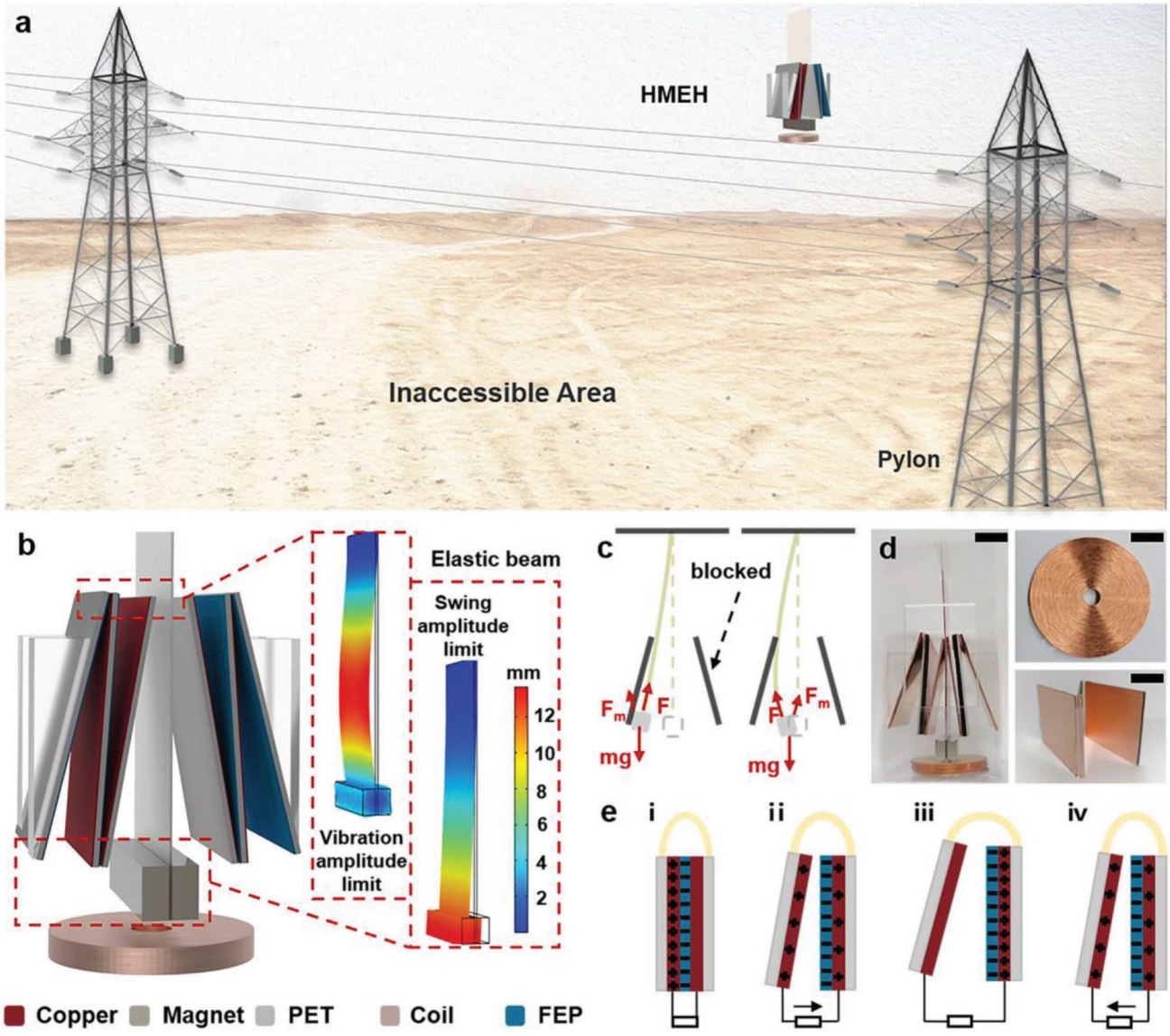

Figure 1. Design and operation of HMEH. a) Schematic diagram of the operating environment of the HMEH. b) Structure and materials design of the HMEH device. Motion state of the elastic beam. c) Stress diagram of the flexible beam. d) Photographs of the HMEH device, the Cu coil used by EMGs, and the multilayered TENG. (Scale bar is 1 cm). e) Working mechanism of each TENG unit.

and finally vanishes. At the end of the latter process, the net force is only the gravity (Figure S2iv, Supporting Information), and the tribo-layers separate (see Video S2 and Figure S3, Supporting Information, for the details of the whole process).

Figure 2b exhibits a typical waveform of open-circuit voltage (V_{oc}) as a function of time for one multilayered TENG during its contact–separation within one swing motion. This could be linked to the simulation results of Figure 2a as follows. In the initial phase (Figure 2a-i), when the pendulum swings toward the multilayered TENG unit, tribo-layer A is hit by the pendulum and contact tribo-layer B, with the electric potential becoming slightly positive on the tribo-layer A side and slightly negative on the tribo-layer C side (Figure 2a-i), accounting for the first voltage oscillation (Figure 2b-i). The subsequent motion of the pendulum forces the block of tribo-layer A and tribo-layer B toward tribo-layer C (Figure 2a-ii), leading to the second voltage oscillation (Figure 2b-ii). At the end of this full contact, momentarily electric potential changes become negligibly small (Figure 2a-ii). Right after that, the tribo-layer A impacts the pendulum that just started its vibration, making it rapidly hit the tribo-layer B and bounce back. The hit-and-bounce back process happens four times, generating four peaks in the waveform (Figure 2b-iii) due to large impulse during the process, which is reflected as large electric potential changes in simulation results (Figure 2a-iii). As the pendulum loses its contact with gradually decreasing tension force, it moves to the opposite direction under the action of gravity, which eventually leads to a decline of V_{oc}, (Figure 2b-iv) while the electric potential stays the same as before (Figure 2a-iv) compared to the previous phase. Additionally, there are asymmetries in the

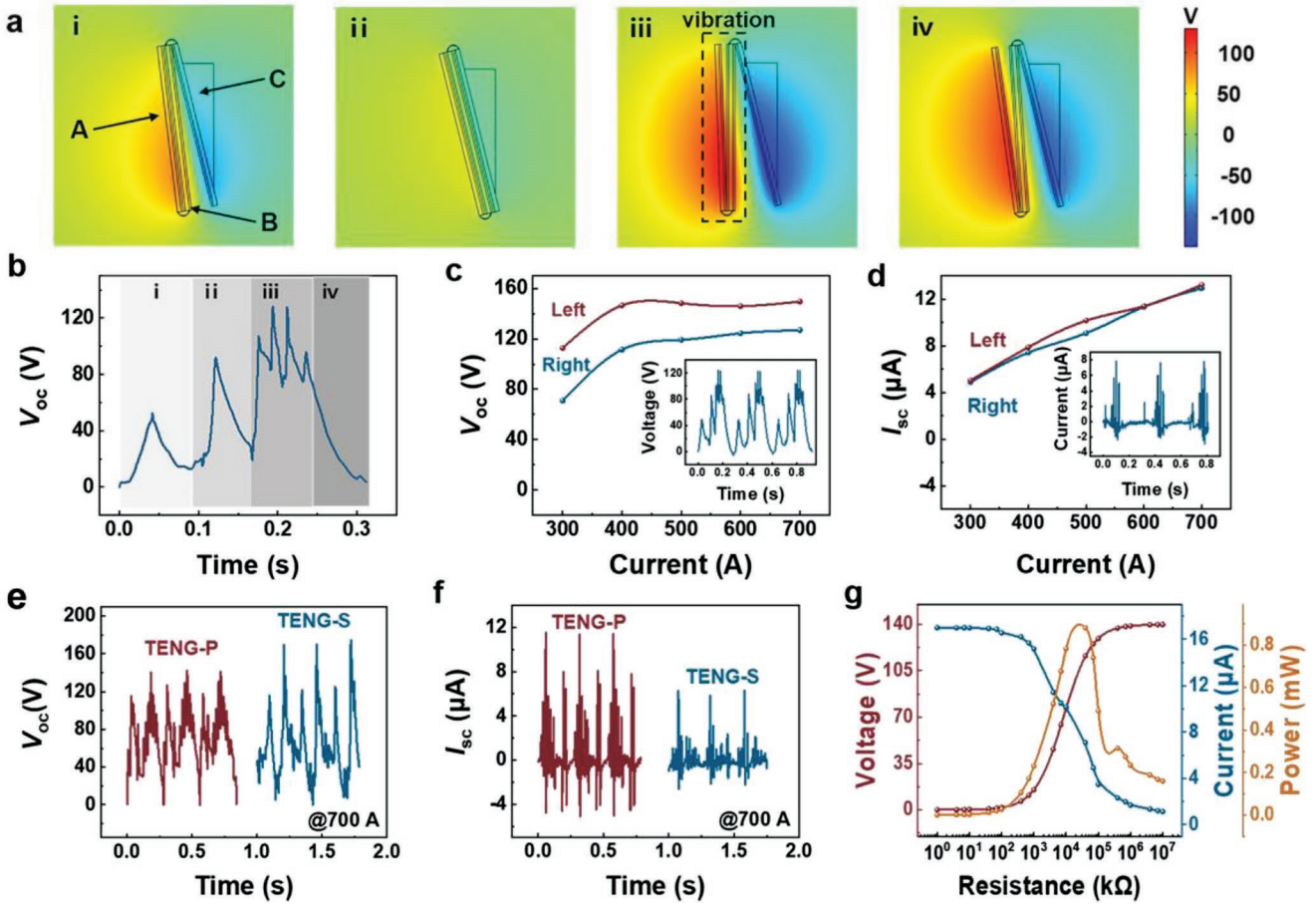

Figure 2. Output performance of the TENG unit in HMEH. a) Potential simulation results of four typical states in the working process. b) Typical waveform of the single TENG unit. c) Open-circuit voltage and d) short-circuit current of TENG unit on both sides. Insets are the typical output performance of the right TENG unit under the current intensity of 600 A. e) Open-circuit voltage and f) short-circuit current of two TENG units connected parallel and series. g) Output voltage, current, power of the TENG units connected in parallel under variable load resistance.

V_{oc} waveform of Figure 2b, namely in phases ii–iii it rises more swiftly than it decays. This can be qualitatively understood in terms of variations in impulse.

To obtain the optimized wave form of the HMEH of Figure 2b, it was necessary to elaborate on the role of forces and momenta acting on the TENG unit, which are due to the gravity provided by the pendulum unit, which contains magnet blocks and the magnetic force of the EMG unit (Figure S2, Supporting Information). To identify their roles, the swing motion of the pendulum that directly determines the output performance of the HMEH needs particular attention. It was found that the size of magnets has a much more obvious effect than their mass (Figure S4, Supporting Information). The swing frequency is approximately inversely proportional to the mass of the pendulum, while the output voltage increases with mass (Figure S4b, Supporting Information), and larger the mass of the magnetic block means larger the momentum acting on the TENG unit. However, it was also found that mass variation affects only the amplitude; the wave form stays the same; and as the size of the magnets was increased, vibrations became more chaotic, implying the momentum due to the magnetic force increases with the size of the magnetic block, as the magnetic force is in multiple directions which causes irregular waveforms (Figure S4c, Supporting Information). Therefore, for an optimized signal, magnets with a mass of 26.25 g for charging 10 μF capacitor (Figure S4d, Supporting Information) and a 28.79 g mass (a mass comparable to the mass of the magnet) for the pendulum (Figure S5, Supporting Information) were chosen. Furthermore, another limiting factor on force and momentum is the lay angle (θ) of the multilayered TENG, which consequently influenced the output. The output voltage reached the maximum value at 14° (Figure S6, Supporting Information). The distance (*d*) between the upper edge of the multilayered TENG and the pendulum got smaller when θ changed from 10° to 18°, and the swing frequency gradually increased. Because the tilted TENG blocked the middle part of the pendulum, the bottom half of the pendulum got bent at a greater angle and moved faster. For small angles (10°, 12°), *d* exceeded the vibration amplitude of the pendulum so that the TENG unit cannot support the middle part, and the bottom half cannot push two tribo-layers to make full contact. Also, the upper edge blocked the pendulum at 16° and 18°, preventing the bottom half from overcoming its damping force and forcing the second TENG unit to contact and separate.

We need to emphasize that we chose a multilayered TENG unit that has three layers (TENG-M) instead of double-layer TENG (TENG-D), even though the electric potential simulations were similar (Figure S7 and see Note S2, Supporting Information, for parameter setting of the simulation calculation of TENG-D) and the TENG-D yielded larger V_{oc} compared to TENG-M for a fixed current intensity of transmission lines of 700 A (Figure S8a, Supporting Information). However, the short-circuit current (I_{sc}) of TENG-M is larger than that of TENG-D (Figure S8b, Supporting Information). The reason behind this can be understood as follows. The addition of one more layer to TENG-D to make a TENG-M decreases the d and increases the swing frequency of the pendulum (Figure S8c, Supporting Information). As a result, charging a 10 μF capacitor can be much more efficient for TENG-M (Figure S8d, Supporting Information). The above mentioned suggests that multilayered TENG improves the output, from which it can be deduced that adding more TENGs may further enhance the output.

One direct consequence of the swing frequency of the pendulum, which is the determining factor of varying magnetic force and the accompanying impulse, is the unusual behavior of I_{sc} of TENG-M. The output performance of the TENG-M was studied under various current intensities, and it was found that except for 300 A, the waveforms and peak-to-peak values of V_{oc} are the same (Figure S9a, Supporting Information). In contrast, the peak-to-peak values of I_{sc} exhibited a linear increase with increasing current intensities by keeping the same I_{sc} wave pattern (Figure S9b, Supporting Information). This is a manifestation of a critical magnetic force (corresponding to a current intensity between 300 and 400 A) acting on the TENG-M via the pendulum unit, above which there is a saturation of V_{oc} due to maximized triboelectrification. However, the I_{sc} is expected to amplify as charges driven per unit time in tribo-layers of TENG-M increase due to increasing impulse.

Figure 2c,d displays the V_{oc} and I_{sc} of each TENG unit on both sides (insets are the typical waveforms). The corresponding current output performance of the two multilayered TENG is similar, but the voltage output differs. Because the TENG unit operated in contact–separation mode is considered a resistor connected in parallel with the current source and series with the capacitor in the equivalent circuit model. There may be some differences in device fabrication that result in inconsistent parameters, causing a voltage difference. Here, to contrast the circuit connection mode of two multilayered TENGs whose working state was opposite, they were connected in parallel and series (recorded as TENG-P and TENG-S) to test the output. The V_{oc} of TENG-P is lower (Figure 2e) but a substantially great I_{sc} (Figure 2f), indicating that they do not have a linear relationship. Because the internal current source of a TENG unit is not ideal, the resistance varies as the capacitance changes greatly. Consequently, the performance of current sources in parallel increases, whereas the performance of a series setup is roughly equal to the performance of the best current source. In addition, two multilayered TENGs contact and separate successively. The waveform of V_{oc} is similar, but there is a phase difference (Figure S10a, Supporting Information). As a result, the TENG may charge each other when connected in series for the capacitance properties so that the current waveform of TENG-S does not get multiple peaks. The output of TENG-P gradually increases as the excitation current intensities rise (Figure S10b, Supporting Information). As a result, we tested the load characteristics under 700 A to obtain the maximum instantaneous power output of the TENG-P and TENG-S (Figure S10c, Supporting Information). Multilayered TENGs were chosen to be connected in parallel to get a superior output characteristic, with a minor matched resistance of 40 MΩ and a greater output power of 0.88 mW. The V_{oc} gradually increased and became saturated from low resistance to high resistance. Also, the I_{sc} represented an opposite trend (Figure 2g).

2.3. EMG Response of HMEH

The subsequent optimization of EMG impacts the overall output of HMEH. The magnetic field distribution in the air domain was determined using the Gauss theorem. **Figure 3**a demonstrates the magnetic induction line distribution of the magnets in a typical state (inset is a physical picture of the Cu coil). The direction of magnet magnetization is perpendicular to the direction of the pendulum. The electromagnetic induction effect converts the movement of permanent magnets into electricity. Besides, the magnetic flux produced by the transmission line also has an essential impact on the output of the EMG. Hence, coil placement was discussed to integrate the TENG and EMG units effectively. The coil was placed at the bottom and side of the shell (recorded as EMG-B and EMG-S). For the EMG-B, the magnets slide back and forth over the coil. As the magnet moved on both sides from the middle of the coil, the magnetic flux gradually decreased. Then the magnet returned to the middle of the coil, and the flux gradually increased. By contrast, when the magnets moved toward and away from the coil, the magnetic flux passing through the EMG-S only changed once, resulting in a smaller induction electric potential. COMSOL software was used to calculate the magnetic flux passing through the copper coil (Figure 3b), contributing to exploring the output of two coils with distinct generation mechanisms. That is, the output frequency of the EMG-B was twice that of the EMG-S. From the waveforms of a typical output parameter from both coils (Figure S11a,b, Supporting Information), the output performance of EMG-B was much higher than that of EMG-S, further indicating that EMG-B was superior.

The dependence output V_{oc} and I_{sc} of each EMG unit on the current intensity has been measured (Figure S11c,d, Supporting Information), which is determined by the variable rate of magnetic flux. The magnetic flux is contributed by the magnets and the alternative magnetic field. The increased current intensity increases the magnetic field strength, enhancing the EMG output. Also, the increased current intensity improves the swing frequency, which positively affects the output performance of the EMG. The output peak power of both EMG units is shown in Figure S11e, Supporting Information. The highest peak powers are 12.2 and 3.7 mW, respectively, with a loading resistance of 496 Ω. The output voltage and current of EMG-B with different resistances were also measured under the current intensity of 700 A. As displayed (Figure S11f, Supporting Information), the V_{oc} of EMG-B increases with the considerable external load resistance, whereas the I_{sc} decreases with the resistance increase, respectively.

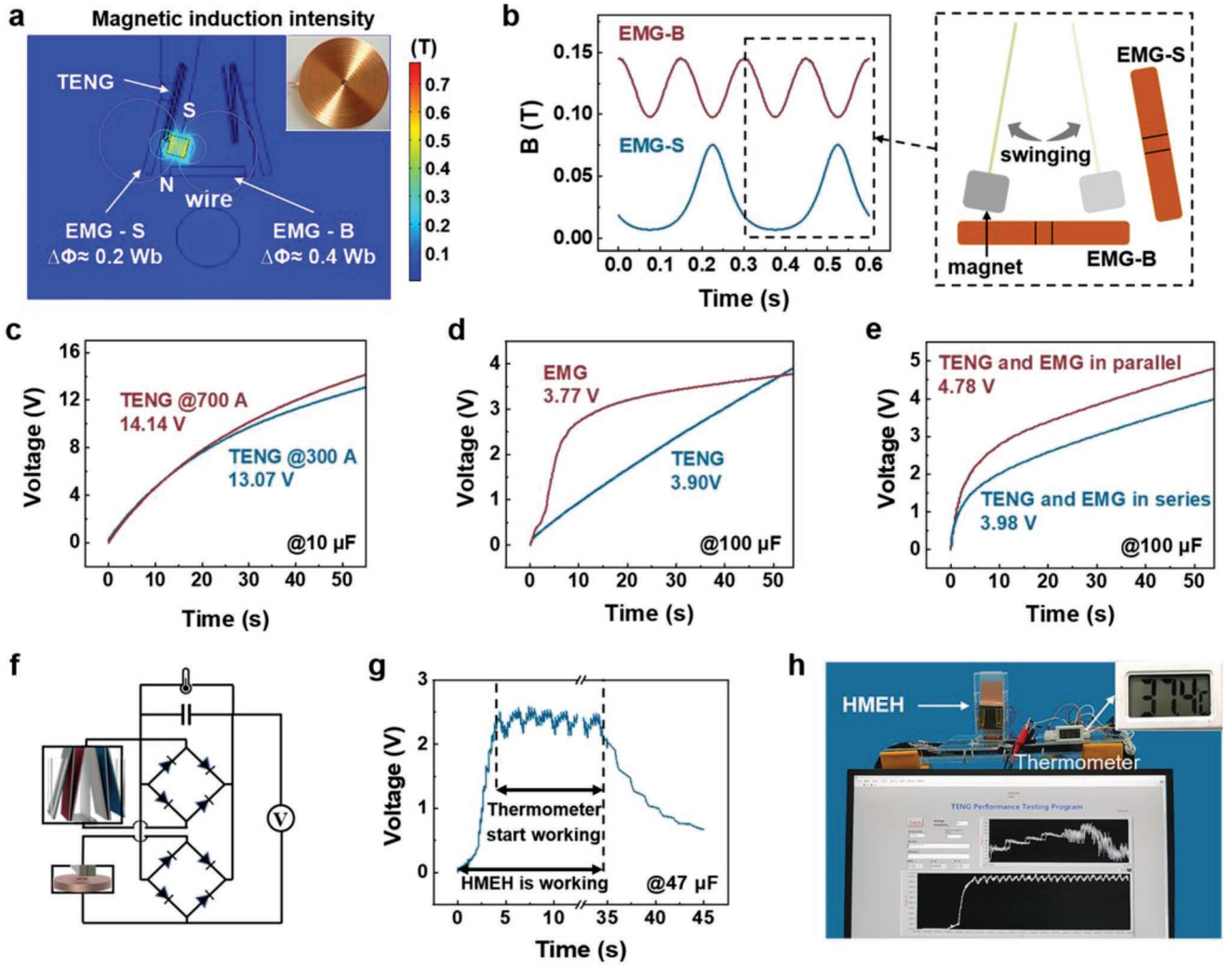

Figure 3. Output performance and application of the HMEH. a) Simulation results of the magnetic distributions in a typical state. Inset is the sketch of the Cu coil. b) Waveform of the two EMG with the motion of the magnet. c) Charging voltage curves for 10 μF capacitor under different current intensities. d) Charging voltage curves for 100 μF capacitor by TENG and EMG. e) Charging characteristics of the TENG and EMG are connected in parallel and series. f) Schematic diagram of a circuit powering a thermometer. g) Typical working waveform of the thermometer. h) Photograph of powering the thermometer.

There is a distance between the magnets and the transmission line, where the coil is inserted. Since the installation configuration of magnets and coils enables the coils to cut the magnetic flux lines to a maximum degree, the volume of the coil has a significant impact on the output. When the dimension is determined by the swing amplitude (2 cm), the coil with a suitable thickness may obtain the highest output performance. COMSOL software based on the finite-element simulation was used to simulate the induced voltage in the Cu coil (Figure S12a, Supporting Information), which continues to rise as the thickness increases. The relative displacement of the pendulum and the distance between the magnet and the wire is presented in Figure S12b, Supporting Information. The displacement of the pendulum decreases with the increase of the distance. When it exceeds 4 mm, the pendulum cannot push the multilayered TENG to contact completely, causing a low output (Figure S12c, Supporting Information). The coil thickness is 4 mm to achieve the best possible balance between the two HMEH modules.

Several capacitors were charged to study the charging characteristics roundly. Figure 3c describes the charging voltage curve of the TENG module, in which the 10 μF capacitor could be charged to exceed 13 V under different current intensities. Other capacitors showed similar charging results (Figure S13a, Supporting Information). The voltage of capacitors charged for 55 s under different current densities was close, which indicated that the TENG module has a relatively stable output in terms of charging capacitors. Figure 3d demonstrates the charging voltage curve of the 100 μF capacitor by the TENG and EMG modules under the current intensity of 700 A. In the early stage of charging, the EMG could quickly charge the capacitor to a relatively high value, but the charging rate was slow in the later stage. While the TENG maintained a relatively stable rate, the maximum value of EMG was even smaller than TENG after 55 s of charging. The difference in the charging voltage curve became more obvious when using a 10 μF capacitor. While the TENG module continuously charged the

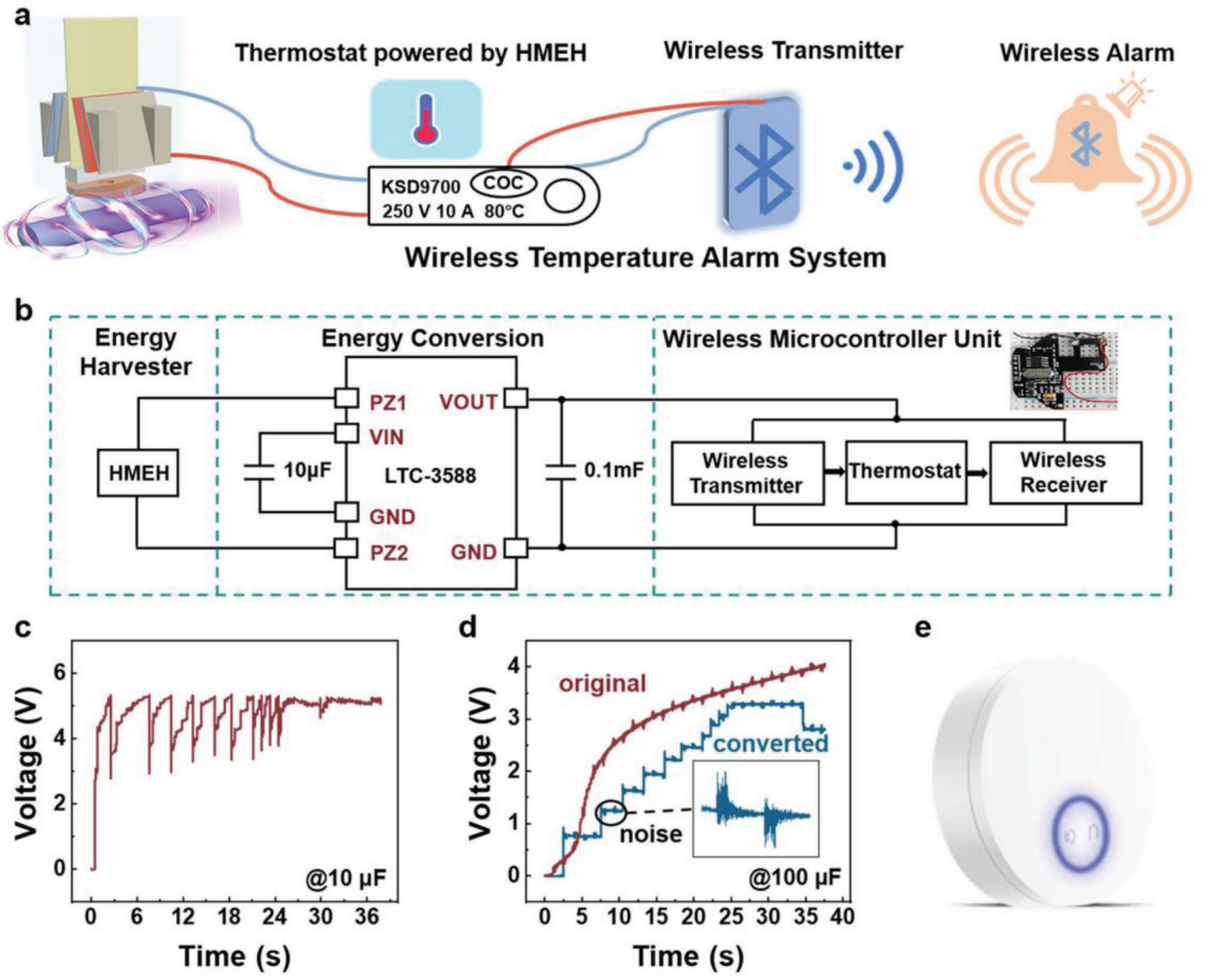

Figure 4. a) Conceptual schematics of the self-powered wireless temperature alarm system. b) A circuit diagram of the HMEH-based self-powered wireless temperature alarm system. The inset shows a photograph of the wireless transmitter. c) The waveform of the charging process of the 10 μF capacitor. d) The waveform of the original and converted charging process of the 100 μF capacitor. e) Photograph of the wireless alarm device.

capacitor, the capacitor was rapidly charged to the maximum value by the EMG module. After charging simultaneously, the value of TENG was much larger than that of EMG (Figure S13b, Supporting Information). Because the peak V_{oc} value limited the maximum charging voltage of EMG, the peak V_{oc} showed a noticeable decrease after rectification, ≈0.7 V. Although the large I_{sc} of the EMG module provided a fast-charging speed, it cannot charge capacitors persistently. Therefore, the EMG cannot perform stable charging with varying current intensities. Figure 3e and Figure S13c, Supporting Information, display the charging voltage curves when the TENG and EMG modules are specified to connect in parallel and series, respectively. Three capacitors showed the same charging characteristics. Whether the TENG and EMG connected in parallel or series can charge the capacitor to a large value in a short time, and the capacitor could be continuously charged. Both connection modes improved the charging characteristics, and the maximum charging voltage of the parallel connection performed better.

2.4. Applications of HMEH

Figure 3f displays the schematic diagram of a thermometer powered by the HMEH device under the current intensity of 700 A to detect the temperature through charging a capacitor of 47 μF. The typical working waveform for the capacitor to power the thermometer is plotted in Figure 3g. After the capacitor was charged to 2.5 V in 5 s, the switch was turned on, and the thermometer connected to the circuit. The thermometer could continuously work and display the temperature (Figure 3h), and the charging voltage remained steady at 2.4 V, which ensured the stable operation of the thermometer. The complete charging and discharging process of the capacitor and the working process of the thermometer are recorded in Video S3, Supporting Information.

Figure 4a shows an application concept of self-powered wireless alarm systems. The HMEH device can generate electric energy under an AC magnetic field to activate a thermostat. When the temperature is higher than the trigger threshold of the thermostat, the wireless transmitter device can transmit a

signal of a control command to the wireless receiver, and the alarm will ring to remind the maintenance personnel. This type of system offers an early warning function to avoid fire disasters, and it can implement other functions by changing the thermostat switch to another switch. Figure 4b plots the logic design of the system. The system comprises the HMEH, wireless microcontroller unit (inset of Figure 4b), and a power managing circuit. The power managing circuit comprises a voltage regulating capacitor (10 μF), a storage capacitor (100 μF), and a Linear technology LTC-3588 circuit. First, the electric energy accumulated in the voltage regulating capacitor until the stored charge could be transferred to the storage capacitor (Figure 4c). Then the storage capacitor was gradually charged to the working voltage. Note that the output voltage was set to 3.3 V by changing the pin of the LTC-3588.

After operating the HMEH under the current intensity of 700 A, the storage capacitor was charged from 0 to 3.3 V within 26 s, and the wireless transmitter was ready to work. When the transmitter started to work, the voltage in the storage capacitor dropped, indicating the wake-up of the transmitter. The wireless alarm emitted light and voice (Figure 4e), and the performance of the temperature alarm system was verified as in Video S4, Supporting Information. Figure 4d exhibits the original charging voltage curve, which seems better than a power managing circuit. In addition, the energy conversion process of the HMEH causes a considerable energy loss because the LTC-3588 is not designed for the HMEH. However, the high voltage in the capacitor may short-circuit the internal electronic circuit of the transmitter without the power managing circuit, and the output of HMEH cannot be directly applied in commercial electronics, so the use of the LTC-3588 is necessary. This demonstration verifies that the HMEH can continuously supply sufficient electric power to the alarm system without an external power source.

3. Conclusion

In summary, we have demonstrated the HMEH device for magnetic energy harvesting based on TENG and EMG modules, used as a power source for wireless monitoring of transmission lines. The device has a simple structure design of magnets attached to the flexible pendulum. The magnets respond to the alternating magnetic field and act as an essential part of the EMG unit. The flexible pendulum enlarges the swing amplitude, pushing the multilayered TENG to contact effectively and indirectly intensifying the EMG unit output. Furthermore, the performance of the TENG can be ulteriorly improved by increasing the number of tribo-layers, after the components of the two modules have been optimized to achieve the highest output performance. The matching rectifier bridges connected the TENG and EMG modules in parallel to charge an energy storage unit. The charging rate was significantly accelerated, meaning the integration of TENG and EMG can achieve their complementary strengths. A self-powered wireless temperature alarm system has been built and tested by utilizing a temperature switch, confirming the technical feasibility of the HMEH for condition monitoring. This work may provide a viable strategy for developing a self-powered warning system utilizing magnetic energy.

4. Experimental Section

Fabrication of the Multilayered TENG: Six acrylic sheets (thickness of 1 mm) were cut into 4 cm × 4 cm to serve as the substrate of the multilayered TENG with a laser cutting machine (6090, 31 Degree Technology, Jiaxing, China). Three acrylic sheets were connected in a group using Kapton tape (thickness of 80 μm), then they were folded into a zigzag structure. The Cu foil (4 cm × 4 cm) and an FEP film (30 μm, size of 4 cm × 4 cm) bonded by another Cu foil (4 cm × 4 cm) were adhered to two adjacent intervals of the zigzag structure. The surface between acrylic and FEP-Cu film was attached by a flexible foam (4 cm × 4 cm) since the contact between two tribo-layers can be improved.

Fabrication of the HMEH Device: An acrylic sheet was cut into four 10 cm × 4.5 cm × 3 mm rectangles and two 4.5 cm × 4.5 cm × 3 mm squares to make the shell of the device with the laser cutting machine. A polyethylene terephthalate (PET, 0.5 mm) was chosen to serve as the flexible pendulum, and two magnets (NdFeB N35) were fixed at the bottom of the pendulum. Then two fabricated multilayered structure TENGs were located on both sides of the pendulum at an angle of 15°, and a Cu coil (diameter of 30 mm, the thickness of 4 mm, coil turns of 2000) was placed at the bottom of the shell.

Characterization and Measurement: The HMEH was placed above the copper cable around the alternating magnetic field generated by an alternating current source (AHY-12 series linear AC adjustable constant current source). The electrical output was measured by an electrometer (Keithley 6514 System Electrometer) and a data acquisition card (NI PCI-6255).

Supporting Information

Supporting Information is available from the Wiley Online Library or from the author.

Acknowledgements

The research was supported by the National Natural Science Foundation of China (61503051).

Conflict of Interest

The authors declare no conflict of interest.

Data Availability Statement

The data that support the findings of this study are available from the corresponding author upon reasonable request.

Keywords

electromagnetic generators, flexible magnetic structure, magnetic energy, self-powered system, transmission lines, triboelectric nanogenerators

Received: November 22, 2021
Revised: May 23, 2022
Published online: June 9, 2022

[1] T. Samad, A. M. Annaswamy, *Proc IEEE Inst Electr Electron ENG* **2017**, *105*, 2244.
[2] V. A. Aksyuk, *Nat. Nanotechnol.* **2017**, *12*, 940.
[3] A. A. Shobole, M. Wadi, *Renewable Sustainable Energy Rev.* **2021**, *149*, 111352.

[4] J. Lopez, J. E. Rubio, C. Alcaraz, *IEEE Wireless Commun.* **2021**, *28*, 48.
[5] S. Z. Tajalli, A. Kavousi-Fard, M. Mardaneh, A. Khosravi, R. Razavi-Far, *IEEE Trans. Cybern.* **2021**, *26*, 1.
[6] M. Alonso, H. Amaris, D. Alcala, R. D. Florez, *Sensors* **2020**, *20*, 2187.
[7] Y. Shi, X. Wei, K. Wang, D. He, Z. Yuan, J. Xu, Z. Wu, Z. L. Wang, *ACS Appl. Mater. Interfaces* **2021**, *13*, 50329.
[8] D. K. Sah, T. Amgoth, *Inf. Fusion* **2020**, *63*, 223.
[9] C. Jiang, X. Li, S. W. M. Lian, Y. Ying, J. S. Ho, J. Ping, *ACS Nano* **2021**, *15*, 9328.
[10] Z. Wu, Y. Wen, P. Li, *IEEE Trans. Energy Convers.* **2013**, *28*, 921.
[11] H. Ryu, H. J. Yoon, S. W. Kim, *Adv. Mater.* **2019**, *31*, 1802898.
[12] V. Kashyap, S. Sakunkaewkasem, P. Jafari, M. Nazari, B. Eslami, S. Nazifi, P. Irajizad, M. D. Marquez, T. R. Lee, H. Ghasemi, *Joule* **2019**, *3*, 3100.
[13] S. Yong, J. Wang, L. Yang, H. Wang, H. Luo, R. Liao, Z. L. Wang, *Adv. Energy Mater.* **2021**, *11*, 2101194.
[14] Z. Yuan, X. Wei, X. Jin, Y. Sun, Z. Wu, Z. L. Wang, *Mater. Today Energy* **2021**, *22*, 100848.
[15] X. Wei, Z. Zhao, L. Wang, X. Jin, Z. Yuan, Z. Wu, Z. L. Wang, *Nano Energy* **2022**, *91*, 106652.
[16] Z. Wu, J. Tang, X. Zhang, Z. Yu, *Appl. Phys. Lett.* **2017**, *111*, 013903.
[17] F. Zheng, Y. Sun, X. Wei, J. Chen, Z. Yuan, X. Jin, L. Tao, Z. Wu, *Nano Energy* **2021**, *90*, 106631.
[18] B. Chen, Y. Yang, Z. L. Wang, *Adv. Energy Mater.* **2018**, *8*, 1702649.
[19] W. Liu, Z. Wang, G. Wang, G. Liu, J. Chen, X. Pu, Y. Xi, X. Wang, H. Guo, C. Hu, Z. L. Wang, *Nat. Commun.* **2019**, *10*, 1426.
[20] Y. Wang, Y. Yang, Z. L. Wang, *npj Flexible Electron.* **2017**, *1*, 10.
[21] R. Li, X. Wei, J. Xu, J. Chen, B. Li, Z. Wu, Z. L. Wang, *Micromachines* **2021**, *12*, 352.
[22] Y. S. Choi, Q. Jing, A. Datta, C. Boughey, S. Kar-Narayan, *Energy Environ. Sci.* **2017**, *10*, 2180.
[23] L. B. Huang, G. Bai, M. C. Wong, Z. Yang, W. Xu, J. Hao, *Adv. Mater.* **2016**, *28*, 2744.
[24] Y. Shi, Y. Wang, Y. Deng, H. Gao, Z. Lin, W. Zhu, H. Ye, *Energy Convers. Manage.* **2014**, *80*, 110.
[25] Z. Wu, H. Guo, W. Ding, Y. C. Wang, L. Zhang, Z. L. Wang, *ACS Nano* **2019**, *13*, 2349.
[26] K.-W. Lim, M. Peddigari, C. H. Park, H. Y. Lee, Y. Min, J.-W. Kim, C.-W. Ahn, J.-J. Choi, B.-D. Hahn, J.-H. Choi, D.-S. Park, J.-K. Hong, J.-T. Yeom, W.-H. Yoon, J. Ryu, S. N. Yi, G.-T. Hwang, *Energy Environ. Sci.* **2019**, *12*, 666.
[27] Y. Feng, X. Liang, J. An, T. Jiang, Z. L. Wang, *Nano Energy* **2021**, *81*, 105625.
[28] C. Ye, K. Dong, J. An, J. Yi, X. Peng, C. Ning, Z. L. Wang, *ACS Energy Lett.* **2021**, *6*, 1443.
[29] H. Yang, M. Deng, Q. Tang, W. He, C. Hu, Y. Xi, R. Liu, Z. L. Wang, *Adv. Energy Mater.* **2019**, *9*, 1901149.
[30] H. Yang, H. Yang, M. Lai, Y. Xi, Y. Guan, W. Liu, Q. Zeng, J. Lu, C. Hu, Z. L. Wang, *Adv. Mater. Technol.* **2019**, *4*, 1800278.
[31] M. Li, Y. Jie, L.-H. Shao, Y. Guo, X. Cao, N. Wang, Z. L. Wang, *Nano Res.* **2019**, *12*, 1831.